Physics Letters A 375 (2011) 4007–4021

Contents lists available at SciVerse ScienceDirect

Physics Letters A

www.elsevier.com/locate/pla

On vortex shedding from a hexagonal cylinder

Hatef A. Khaledi *, Helge I. Andersson

Department of Energy and Process Engineering, Norwegian University of Science and Technology, 7491 Trondheim, Norway

ARTICLE INFO

Article history:
Received 1 June 2011
Received in revised form 15 August 2011
Accepted 23 September 2011
Available online 29 September 2011
Communicated by F. Porcelli

Keywords:
Unsteady wakes
Vortex shedding
Hexagonal cylinders
Turbulence

ABSTRACT

The unsteady wake behind a hexagonal cylinder in cross-flow is investigated numerically. The time-dependent three-dimensional Navier–Stokes equations are solved for three different Reynolds numbers *Re* and for two different cylinder orientations. The topology of the vortex shedding depends on the orientation and the Strouhal frequency is generally higher in the wake of a face-oriented cylinder than behind a corner-oriented cylinder. For both orientations a higher Strouhal number *St* is observed when *Re* is increased from 100 to 500 whereas *St* is unaffected by a further increase up to $Re = 1000$. The distinct variation of *St* with the orientation of the hexagonal cylinder relative to the oncoming flow is opposite of earlier findings for square cylinder wakes which exhibited a higher *St* with corner orientation than with face orientation.

1. Introduction

The prototype bluff body is the infinitely long circular cylinder, which has been subjected to numerous theoretical, experimental and computational investigations during several decades. The great variety of studies on the flow past a circular cylinder is evidenced by the comprehensive compilation by Zdravkovich [1] whereas the review by Williamson [2] provides a thorough description of the vortex dynamics in the cylinder wake. Besides its obvious practical relevance in a variety of applications, see e.g. Ref. [1], long uniform cylinder models with a circular cross-section are relatively easy to produce for wind tunnel and towing-tank testing.

The wake flow behind infinitely long sharp-edged bluff bodies may be distinctly different from the wake of a circular cylinder since the flow separation from the former often occurs at the sharp corners. A rectangular cylinder with cross-section with side ratio d/w was considered by Sohankar et al. [3]. Side ratios from 4 to 1 were considered in a series of 2D calculations for Reynolds numbers $Re = 100$ and 200 to investigate the influence of the flow angle of incidence. In the limit as the side ratio d/w tends to infinity, the rectangular cylinder becomes an infinitely thin plate, as considered recently by Narasimhamurthy and Andersson [4]. The special case $d/w = 1$, i.e. a square cylinder, has been extensively studied and is of particular relevance herein since the square cylinder represents a special case of a polygonal cylinder.

Flow past long cylinders with polygonal cross-sections resembles the flow around circular cylinders, but the flow may sometimes detach from the polygon at a sharp corner. Regular polygons with an even number N of sides are the square, hexagon, octagon, decagon, and so on. Almost all investigations of wakes behind polygonal cylinders have been concerned with triangular ($N = 3$) and quadratic ($N = 4$) cylinders. An early experimental study of the latter case was performed by Vickery [5] in the Reynolds number range from $4 \cdot 10^4$ to $1.6 \cdot 10^5$. It was reported that the Strouhal frequency increased modestly as the angle of attack α was increased from 0° to 45°, i.e. from *face orientation* to *corner orientation*. Knauss et al. [6] measured the vortex shedding frequency in the wake of elliptical and square cylinders in the Reynolds number range from 300 to 1200. They argued that the Strouhal number should be based on the height h of the projected cylinder on a plane normal to the flow direction rather than on a geometrical measure d of the bluff body. It turned out that the shedding frequency was almost unaffected by *Re* but the Strouhal number *St* in the case of face orientation ($\alpha = 0°$) was considerably lower than for corner orientation ($\alpha = 45°$). In the latter case *St* was almost indistinguishable from the Strouhal number in the wake behind a 90° wedge and the authors therefore concluded that effects from the afterbody of the square cylinder were negligible. At $Re = 374$ the Strouhal number *St* increased rapidly from 0.14 to 0.18 as α increased from 0° to 10° and thereafter remained almost independent of the angle of incidence. A similar trend was found for $Re = 1215$. The computer simulations at $Re = 200$ reported by Sohankar et al. [7] showed that *St* increased gradually from ca 0.17 to above 0.20 in the interval from $\alpha = 0°$ to 45°. The different *St* variation in the 2D computations and the experiments was ascribed to the turbulent inflow conditions in the latter. However, the physical realism of 2D calculations is questionable since a transition from 2D to 3D wake dynamics occurs already at $Re \sim 160$,

* Corresponding author.
E-mail address: hatef.khaledi@ntnu.no (H.A. Khaledi).

0375-9601/$ – see front matter
doi:10.1016/j.physleta.2011.09.046

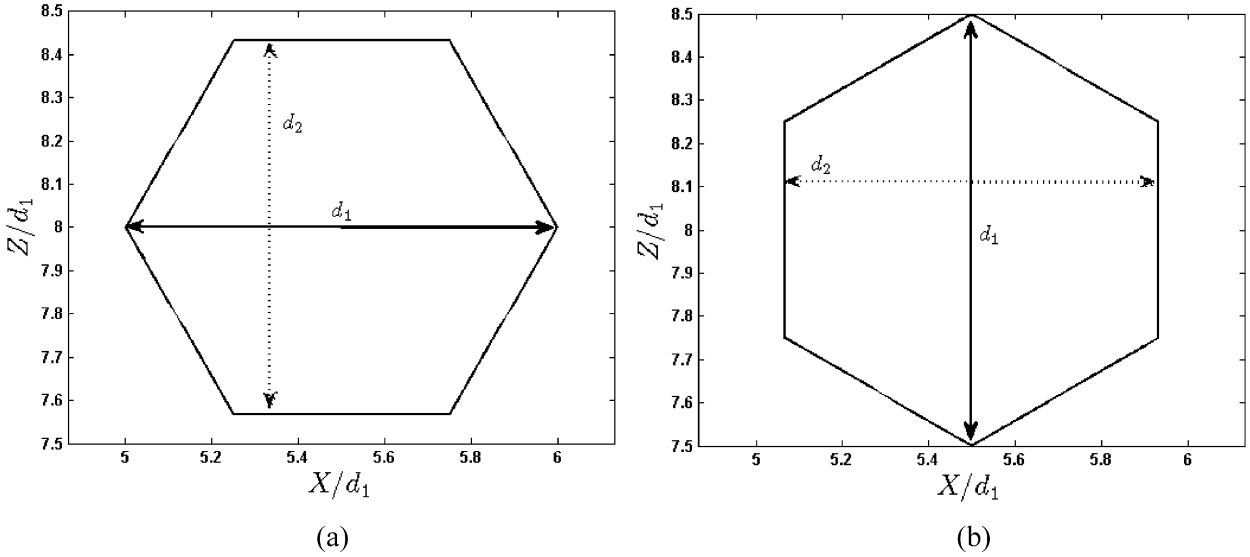

Fig. 1. Two different orientations of the hexagonal cylinder: (a) corner orientation (A), and (b) face orientation (B). The circumscribed diameter $d_1 = 2d$ and the inscribed diameter $d_2 = \sqrt{3}d$ for a regular hexagon with sides d.

as shown by Sohankar et al. [8], Saha et al. [9], and Luo et al. [10]. Such transitions have been extensively explored in wakes of circular cylinders; see e.g. Ref. [2]. The more recent of experimental data of Dutta et al. [11] at Reynolds numbers 1340, 4990, and 9980 seemed to agree with the trend of the Strouhal number variation found by Knauss et al. [6] even though the Strouhal numbers reported in Ref. [11] were based on the side d rather than on the projected height h. Very recently, Yoon et al. [12] found from the Stuart–Landau equation that the critical Reynolds number Re_c for onset of vortex shedding first increased from $Re_c = 45$ for $\alpha = 0°$ and until $\alpha \approx 5°$ and thereafter decreased monotonically to below 40 for $\alpha = 45°$.

The only empirically-based paper on hexagonal cylinders (i.e. $N = 6$) is that by Sparrow et al. [13]. They addressed the heat transfer from some different non-circular cylinders in cross-flow and focused on the crucial role played by choice of the characteristic length in the Nusselt–Reynolds number correlation. Over a wide range of Reynolds numbers above ca 5000, the Nusselt number is higher with face orientation than with corner orientation for cylinders with hexagonal cross-sections. These differences were associated with the differences in the flow patterns for the two orientations. It was assumed that five of the six faces were either fully or partially washed by a recirculation zone in the case of face orientation, whereas only four faces were experiencing flow separation with corner orientation.

With the view to study highway support structures, Bosch and Guterres [14] tested octagonal cylinders ($N = 8$) in a wind tunnel. They found a higher Strouhal number for corner orientation than for face orientation over the Reynolds number range from 5000 to about 20 000 and an accompanying higher drag coefficient. The reported drag coefficients and Strouhal numbers are probably based on the equivalent diameter of the octagonal cross-section although this has not been stated explicitly. Cylindrical models with hexagonal cross-sections were also fabricated but no results were presented in Ref. [14].

Two-dimensional flow past regular polygons at low Reynolds numbers has recently been subjected to an extensive analytical and computational investigation by Tian and Wu [15]. They considered infinitely long cylinders with polygonal cross-sections but only with an even number of faces and only with corner orientation. They argued intuitively that the circular cylinder will be the limiting case as the number of faces N tends to infinity. They therefore generalized the *linear* relationship between St and $Re^{-1/2}$ by Fey et al. [16] into:

$$St_N = \chi(0.2684 - 1.0356\sqrt{\chi/Re}) \tag{1}$$

where $\chi = \chi(N) > 1$ for all polygons. For hexagonal and octagonal cylinders, in particular, χ is 1.0865 and 1.0448, respectively, whereas $\chi \to 1$ as N tends to infinity, i.e. in the limit of a circular cylinder as considered by Fey et al. [16]. The Strouhal number St_N decreases monotonically with N according to Eq. (1) and approaches the Strouhal number for a circular cylinder in the limit as $N \to \infty$. CFD calculations utilizing the commercial Fluent software give results consistent with the formula (1) for $N \geqslant 10$, whereas calculations for $N = 6$ and 8 result in Strouhal numbers below the values given by Eq. (1). The unsteady flow calculations were confined to fairly low Reynolds numbers and no results were provided for $Re > 80$.

The motivation for the present investigation is to consider the flow past a *hexagonal* cylinder which has received only marginal attention so far. The vortex shedding will be explored by means of three-dimensional computer simulations, i.e. direct numerical simulations, for three different Reynolds numbers 100, 500, and 1000. While the lowest Re is in the strictly 2D-shedding regime, the regular shedding is destabilized at $Re = 500$ and turbulence develops at the highest Reynolds number considered. Earlier investigations of flow past cylinders with polygonal cross-sections indicate that the unsteady flow separation and the vortex dynamics in the wake depend on the orientation of the cylinder. To address this aspect, both face orientation and corner orientation of the hexagonal cylinder will be considered.

2. Flow field and computational approach

We consider the flow past an infinitely long straight cylinder with a regular hexagonal cross-section. All six sides of the regular hexagon have the same length d and the interior angles are all 120°. Two different orientations will be considered: the corner orientation (A) and the face orientation (B) shown in Fig. 1. The flow is assumed to be from left to right, i.e. in the positive X-direction. The ratio between the inscribed diameter d_2 and the circumscribed diameter d_1 is 0.866 for a regular hexagon. The circumscribed diameter $d_1 = 2d$ will be used as the reference length scale in the

following, unless otherwise is explicitly mentioned. The axis of the hexagonal cylinder is aligned with the Y-axis of a Cartesian coordinate system and placed at ($X = 5.5d_1$, $Z = 8.0d_1$), as shown in Fig. 1.

The flow is governed by the incompressible Navier–Stokes equations, which are approximated on a staggered Cartesian grid system and solved by the finite-volume solver MGLET developed by Manhart [17] and used, for instance, by Narasimhamurthy and Andersson [4]. The spatial derivatives are approximated by 2nd-order accurate central differences and a 3rd-order Runge–Kutta scheme is used for the time advancement. The Poisson equation governing the pressure field is solved by using the iterative Strongly Implicit Procedure (SIP).

Numerical solutions are obtained on a $20d_1$ long, $16d_1$ high, and $6d_1$ wide computational domain. These measures refer to the size of the domain in the streamwise, transverse, and spanwise directions, respectively. A uniform inflow velocity $U = U_0$, $V = W = 0$ is given at $X = 0$ together with a Neumann condition for the pressure. Free-slip conditions are employed at the upper and lower boundary planes whereas periodicity is imposed at the side-planes of the computational domain. At the outlet boundary Neumann and Dirichlet conditions are used for the velocity components and the pressure, respectively. The Immersed Boundary Method (IBM) described by Peller et al. [18] is used to ensure that no-slip and impermeability along the cylindrical surface are carried over to the structured Cartesian mesh used by MGLET.

Simulations are performed for three different Reynolds numbers $Re = U_0 d_1/\nu$. The computational domain is discretized in $576 \times 80 \times 400$ grid cells for $Re = 100$ and 500, whereas 668 cells are used in the streamwise direction at the highest $Re = 1000$. The time step is set to $\Delta t = 0.001 d_1/U_0$ and the number of pressure iterations at each time step is limited to 30. A doubling of the number of grid points in each coordinate direction is not feasible in this three-dimensional flow problem. However, the two $Re = 100$ cases are re-simulated on a $864 \times 80 \times 434$ mesh and all the gross features observed are indistinguishable from those found using the $576 \times 80 \times 400$ grid cell system.

In order to further justify that the grid resolution is adequate to resolve the turbulence field at the highest Reynolds number, the viscous energy dissipation rate ε is deduced from a simulated flow field. The largest side of each and every grid cell $\Delta = \{\max \Delta X_i\}$ could thus be compared with Kolmogorov's microscale for length $\eta = (\nu^3/\varepsilon)^{1/4}$. The contour plot of the ratio Δ/η in Fig. 2 shows that Δ never exceeds about 2 or 3 times η. This shows that grid resolution used herein is comparable with or somewhat better than in the DNS-study of the wake behind a normal flat plate by Narasimhamurthy and Andersson [4].

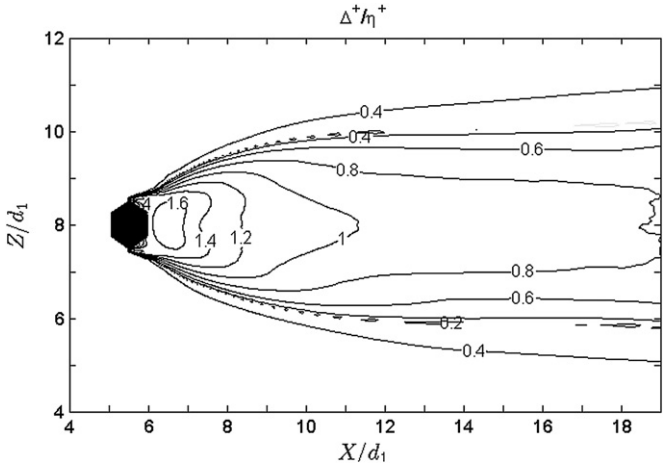

Fig. 2. Estimate of the local relative grid resolution Δ/η in a cross-sectional plane where η is the Kolmogorov length scale. The data are from flow at $Re = 1000$ around a face-oriented (orientation B) hexagonal cylinder.

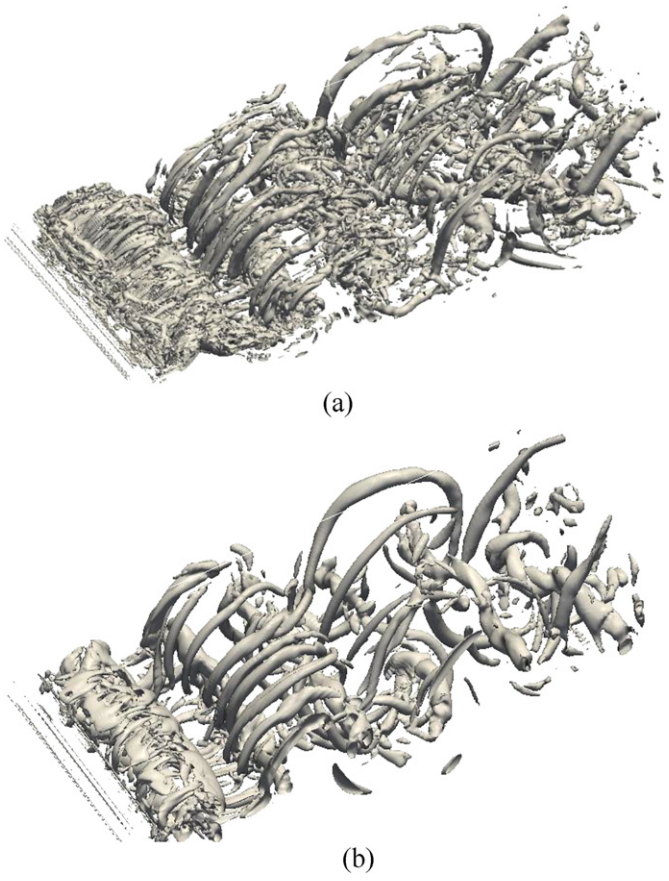

Fig. 3. Isometric view of the wake structure behind the corner-oriented (A) hexagonal cylinder located in the lower left part of the figure: (a) $Re = 1000$, $\lambda_2 = -3$; (b) $Re = 500$; $\lambda_2 = -2.5$.

3. Results and discussions

Results for three different Reynolds numbers 100, 500 and 1000 will be presented both for corner orientation (A) and face orientation (B) of the hexagonal cylinder. First, the focus is on the vortex dynamics in the unsteady wake (Section 3.1) and the instantaneous streamline pattern (Section 3.2), thereafter the shedding frequency is considered (Section 3.3), and finally Reynolds-averaged flow statistics are presented in Section 3.4.

3.1. Vortex dynamics

The vortex structures in the near-wake behind the hexagonal cylinder are visualized by means of λ_2-contours, the definition of which was first proposed by Jeong and Hussain [19]. The scalar λ_2 corresponds to the second largest eigenvalue of the symmetric tensor $S_{ik}S_{kj} + \Omega_{ik}\Omega_{kj}$ where S_{ij} and Ω_{ij} represent the symmetric and anti-symmetric parts of the velocity gradient tensor, respectively. Negative values of λ_2 are associated with low-pressure zones and are normally found in vortex cores. Perspective views of instantaneous λ_2-fields behind the corner-oriented hexagonal cylinder are shown in Fig. 3 for the two highest Reynolds numbers considered. The spanwise-oriented Karman-rollers are clearly identifiable in both plots, together with elongated vortex filaments which are stretched between two consecutive rollers. These streamwise-oriented vortex structures are typical of the mode which occurs

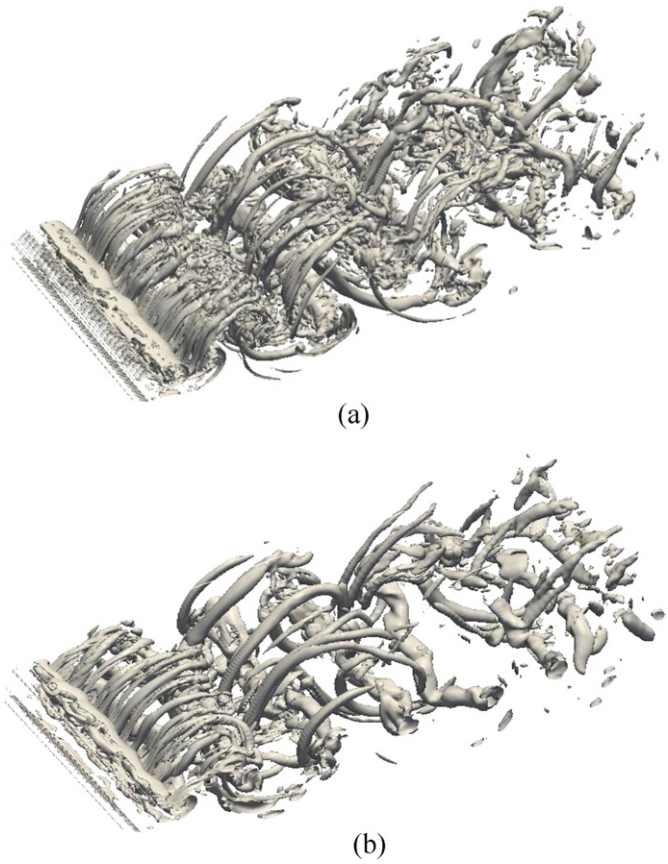

Fig. 4. Isometric view of the wake structure behind the face-oriented (B) hexagonal cylinder located in the lower left part of the figure: (a) $Re = 1000$, $\lambda_2 = -3$; (b) $Re = 500$; $\lambda_2 = -2.5$.

when the nominally two-dimensional vortex shedding undergoes a transition to a three-dimensional flow; see e.g. Williamson [2]. Besides these distinct vortex filaments, the wake at $Re = 1000$ comprises disorderly small-scale vorticity which is almost absent at $Re = 500$. The same Reynolds number effect can be observed from instantaneous vorticity fields in the wake in the lee of the face-oriented hexagonal cylinder in Fig. 4. For a given Re, however, there are no noticeable differences in the wake topology due to the different cylinder orientations in Figs. 3 and 4.

Let us instead consider the instantaneous spanwise vorticity ω_y in a cross-sectional plane as shown in Fig. 5 for all three Reynolds numbers. Laminar shear layers with positive (bright colours) and negative (dark colours) spanwise vorticity develop from the stagnation point at the upstream corner of the corner-oriented hexagon. The thick shear layers at $Re = 100$ remain attached to the body all the way along the flow-parallel faces and separate at the 120° backward-facing steps. The snapshot in Fig. 5(c) shows that the vortices formed in the base region are alternately shed and form a Karman-like vortex street which remains laminar throughout the computational domain.

At $Re = 500$, on the other hand, the shear layers seem to separate somewhere along the flow-parallel faces rather than at the backward-facing corners or vertices. The fairly regular vortices become gradually more destabilized as they are convected downstream. It is noteworthy that a filament with negative spanwise vorticity is entrained into the detaching clockwise-rotating vortex cell (with $\omega_y > 0$) in Fig. 5(b). The instantaneous vorticity contours in Fig. 5(a) suggest that the $Re = 1000$ wake resembles the wake flow at $Re = 500$, although the vorticity field is destabilized already along the flow-parallel faces and the vortices are irregular

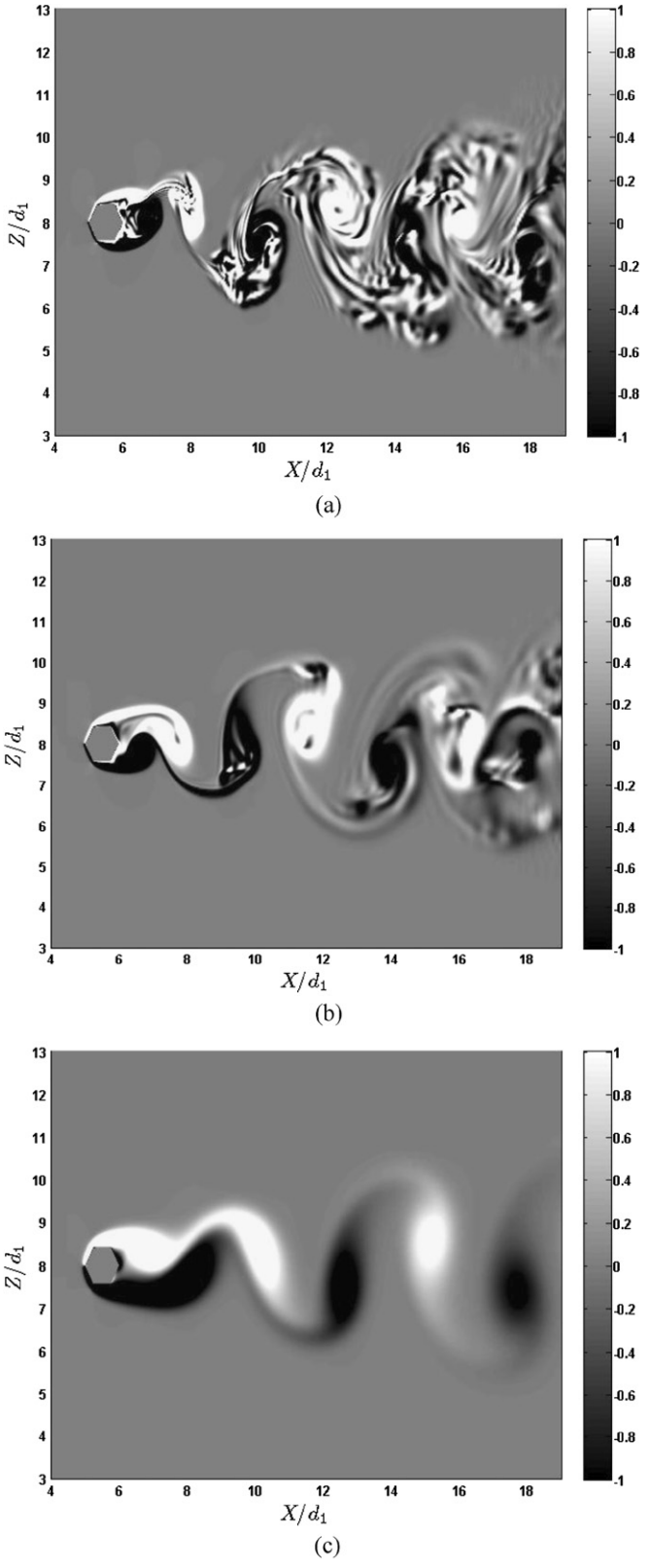

Fig. 5. Instantaneous spanwise vorticity in a cross-sectional (X, Z)-plane behind a hexagonal cylinder with corner orientation (A). (a) $Re = 1000$; (b) $Re = 500$; (c) $Re = 100$. The colour bar refers to the normalized vorticity $\omega_y \nu / U_0^2$ and dark and bright contours refer to negative and positive vorticity, respectively.

from their detachment. The spanwise-oriented vortex cells can still be discerned, but the alternating positive and negative vorticity is blurred by smaller-scale irregularities.

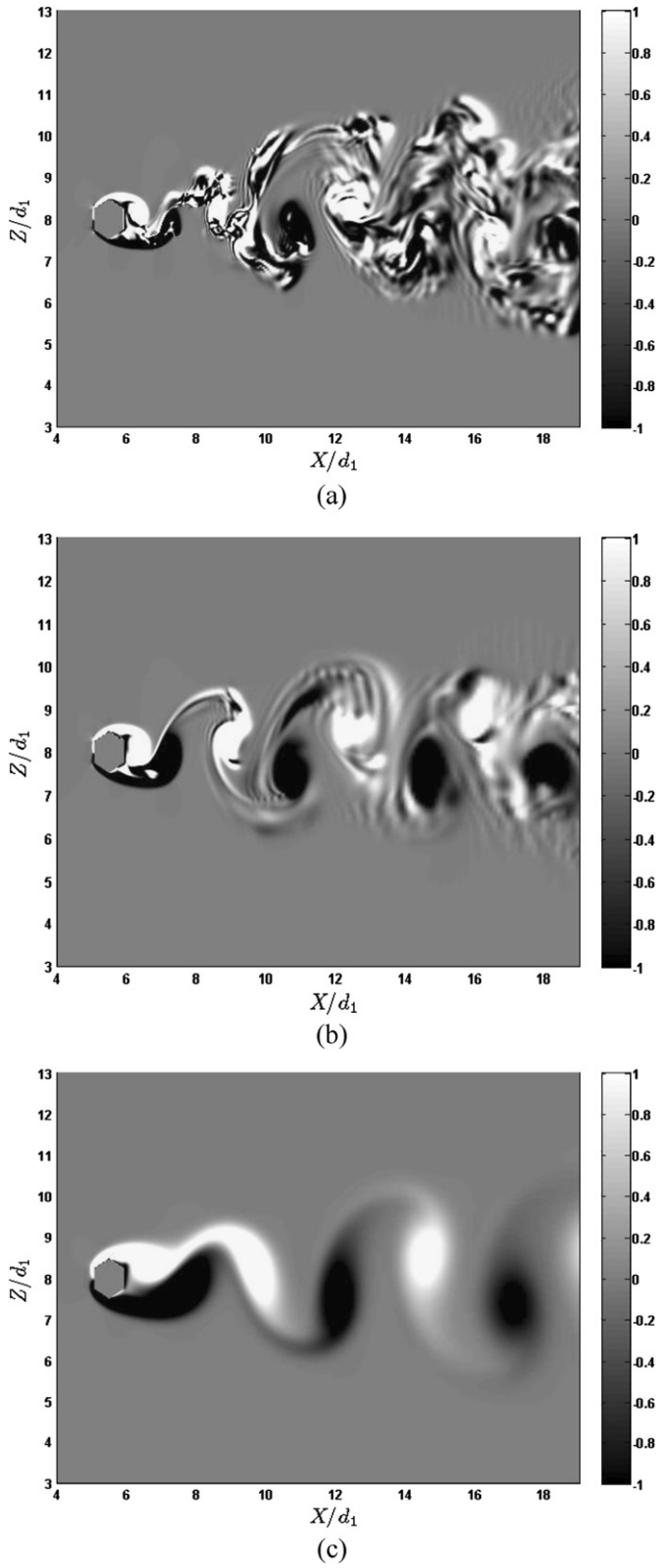

Fig. 6. Instantaneous spanwise vorticity in a cross-sectional (X, Z)-plane behind a hexagonal cylinder with face orientation (B). (a) $Re = 1000$; (b) $Re = 500$; (c) $Re = 100$. The colour bar refers to the normalized vorticity $\omega_y \nu / U_0^2$ and dark and bright contours refer to negative and positive vorticity, respectively.

Almost the same observations can be made from Fig. 6 in which snapshots of the spanwise vorticity for flow along a face-oriented hexagonal cylinder are presented. With face orientation, however, the projection of the cylinder into a plane normal to the flow direction is somewhat wider than for the corner-oriented cylinder; see Fig. 1. Moreover, the edges of the projected cylinder stem from the upper and lower corners of the hexagon. The shear layers which develop from the front stagnation point at the center of the face normal to the free stream, therefore separate from the upper and lower corners for all three Reynolds numbers considered.

3.2. Instantaneous streamline patterns

In order to get an impression of the unsteady shedding behavior, four consecutive snapshots of the streamlines are shown in Fig. 7 for the corner-oriented hexagonal cylinder at $Re = 100$. The focus is on the very-near-wake, loosely termed the *base region* by Lyn et al. [20], which comprises the first four diameters of the wake. The plots are separated $1.8d_1/U_0$ in time and the sequence from Fig. 7(a) to Fig. 7(d) covers almost one shedding cycle. The shedding period will later be shown to be $\approx 5.5d_1/U_0$ for this case (see Section 3.3). In Fig. 7(a) a counter-clockwise vortex has developed at the lower rear face whereas a clockwise vortex can be observed $1.3d_1$ downstream of the rear corner. A saddle-point (S), characterized by the intersection of streamlines, is seen below the center of the clockwise vortex, whereas a wide alleyway flow transports fluid from the lower part of the wake to the upper side and thus contributes to high mixing in the base region. $1.8d_1/U_0$ later, i.e. in Fig. 7(b), the counter-clockwise vortex has grown and detached from the lower rare face and a new clockwise vortex is developing at the upper rare face. The alleyway stream in between the two vortices has now been reversed and a new saddle point has emerged above the counter-clockwise vortex. In Fig. 7(c), the clockwise vortex is at the verge to separate from the upper rare face, whereas a reversed flow driven by this vortex impinges on the lower rare face. No saddle points are visible at this moment of time. The streamline pattern in Fig. 7(d) is almost a mirror-image of the plot in Fig. 7(b). The time sequence shows that the vortices in the wake behind a corner-oriented hexagonal cylinder form as a recirculation bubble at one of the rear faces, before it grows and detaches from the body. An oppositely rotating vortex is then formed at the other rear face, grows and leaves the cylinder.

The center of a vortex can be traced in time and the trajectories of a clockwise and a counter-clockwise vortex are shown in Fig. 8. The data have been extracted from ten snapshots separated $0.6d_1/U_0$ in time. The vortices which develop at either of the two rear faces of the hexagon are seen to drift towards the geometrical symmetry plane $Z/d_1 = 8$ and the two trajectories meet about $1.1d_1$ downstream of the rear corner of the hexagon. In the wake behind a square cylinder at a substantially higher Reynolds number Lyn et al. [20] observed a tendency of the shed vortices to drift away from the symmetry plane downstream of the base region. Although the vortex centers were closer to the geometrical symmetry plane in the base region, the vortices did never reach that plane [20].

At $Re = 500$ the wake has become distinctly three-dimensional, as shown in Fig. 3(b) and true streamlines can no longer be defined. The streamlines of the projected velocity field into the (X, Z)-plane shown in Fig. 9 should therefore be interpreted with some care. It is evident, however, that the flow now separates near the leading edge of the flow-parallel faces, contrary to the situation at $Re = 100$ where the flow separated from the trailing edges of the flow-parallel faces. A distinct upward alleyway flow between the cylinder and the clockwise vortex can be observed in Fig. 9(b) and a corresponding downward flow is seen in between the counter-clockwise vortex and the body in Fig. 9(d).

Let us now consider the flow in the base region of a face-oriented (B) hexagon. For Reynolds number $Re = 100$, the streamlines in Fig. 10(a) show a counter-clockwise separation bubble

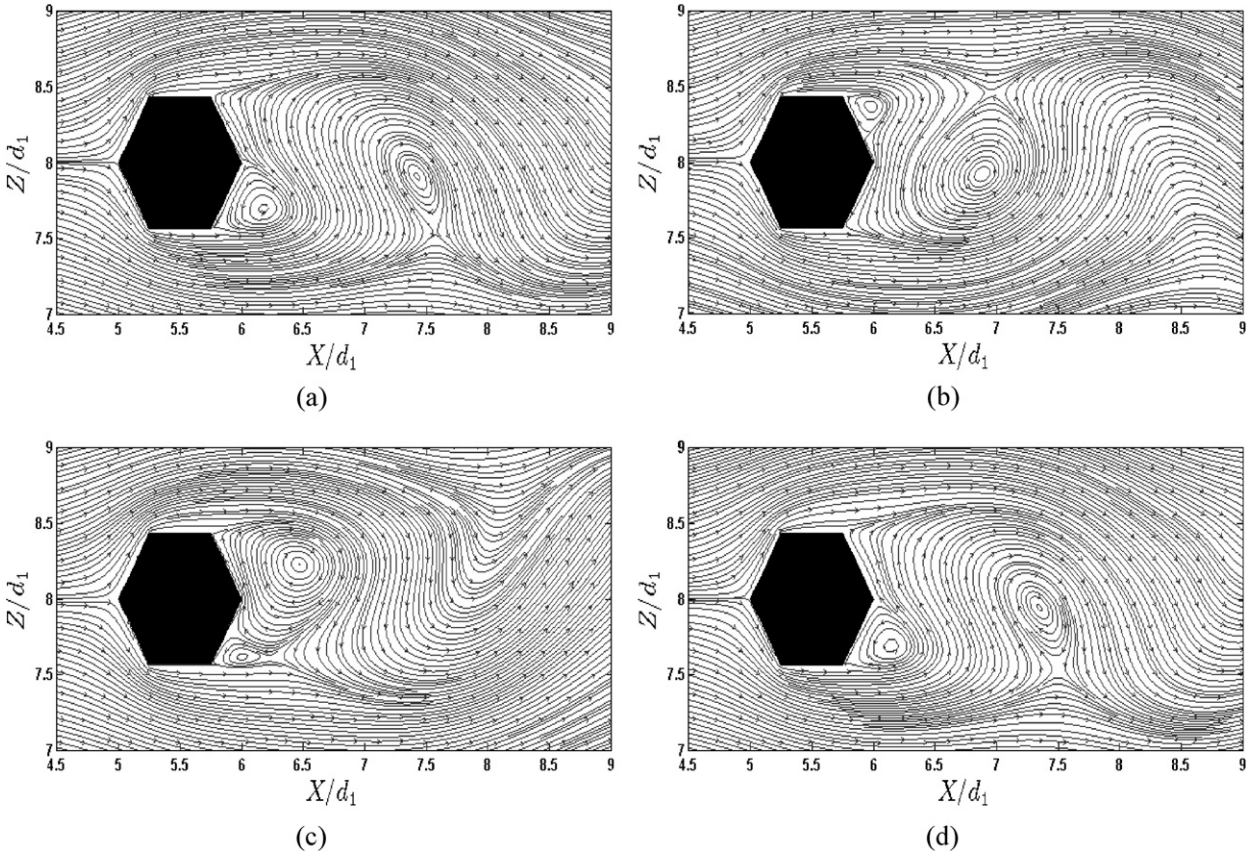

Fig. 7. Instantaneous streamlines for flow around the corner-oriented cylinder (A) at $Re = 100$. The plots are separated $1.8d_1/U_0$ in time.

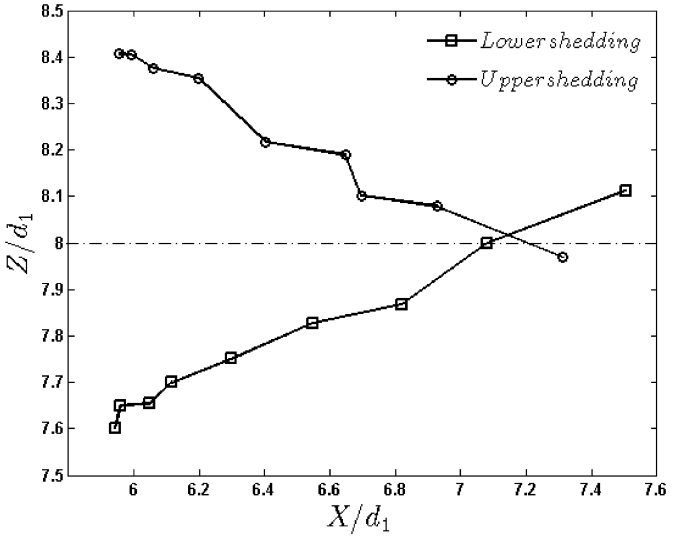

Fig. 8. Trajectories of the vortex centers downstream of the corner-oriented cylinder (A) at $Re = 100$.

at the lower rear face together with a full-blown vortex cell with clockwise rotation about $1d_1$ downstream of the base of the hexagon. An alleyway flow is directed upwards in the base region and a saddle point is seen below the clockwise vortex. $1.8d_1/U_0$ later, this vortex occupies most of the base region and a clockwise recirculation zone emerges at the upper rare face. In Fig. 10(c), the clockwise vortex has grown and is about to detach from the cylinder while at the same time moving downwards into the base region. The snapshot in Fig. 10(d) is taken $5.4d_1/U_0$ later than that in Fig. 10(a) and the streamline patterns in the two plots are quite similar. Also in the case of face orientation, the detached vortices are moving towards the plane of symmetry, as seen in Fig. 11.

The sequence of projected streamlines in Fig. 12 show that the flow at $Re = 500$ separates from the upper and lower corners, similarly as for $Re = 100$. This observation contrasts with the findings for the corner-oriented cylinder. In that case, the location of flow separation was severely affected by the Reynolds number. Irrespective of the actual orientation, however, a more complex streamline pattern is observed at $Re = 500$ than for $Re = 100$.

3.3. Frequency analysis

The instantaneous velocity components U, V, W and also instantaneous pressure, P, were sampled along a line parallel to the axis of the hexagon at $X = 9.5d_1$ and $Z = 6.5d_1$, i.e. $4d_1$ and $-1.5d_1$ offset from the cylinder axis in the streamwise and transverse directions. Representative time traces of W for corner orientation (A) and face orientation (B) are shown in Figs. 13 and 14, respectively. The total time lapse $100d_1/U_0$ comprises 100 000 time steps and covers roughly 20 shedding cycles. One-dimensional energy spectra were obtained from the time history of the cross-stream velocity component W. The spectrum is the Fourier transform of the time-trace signal where the spectral estimator for a finite-length time record is:

$$E(f) = \frac{\hat{W} \times \hat{W}^*}{T}. \tag{2}$$

The superscript $*$ denotes the conjugate of the Fourier-transformed velocity component. The most dominant frequency f is associated with the large-scale shedding of Karman cells.

The Strouhal number is a dimensionless measure of the frequency of the vortex shedding normalized with a characteristic

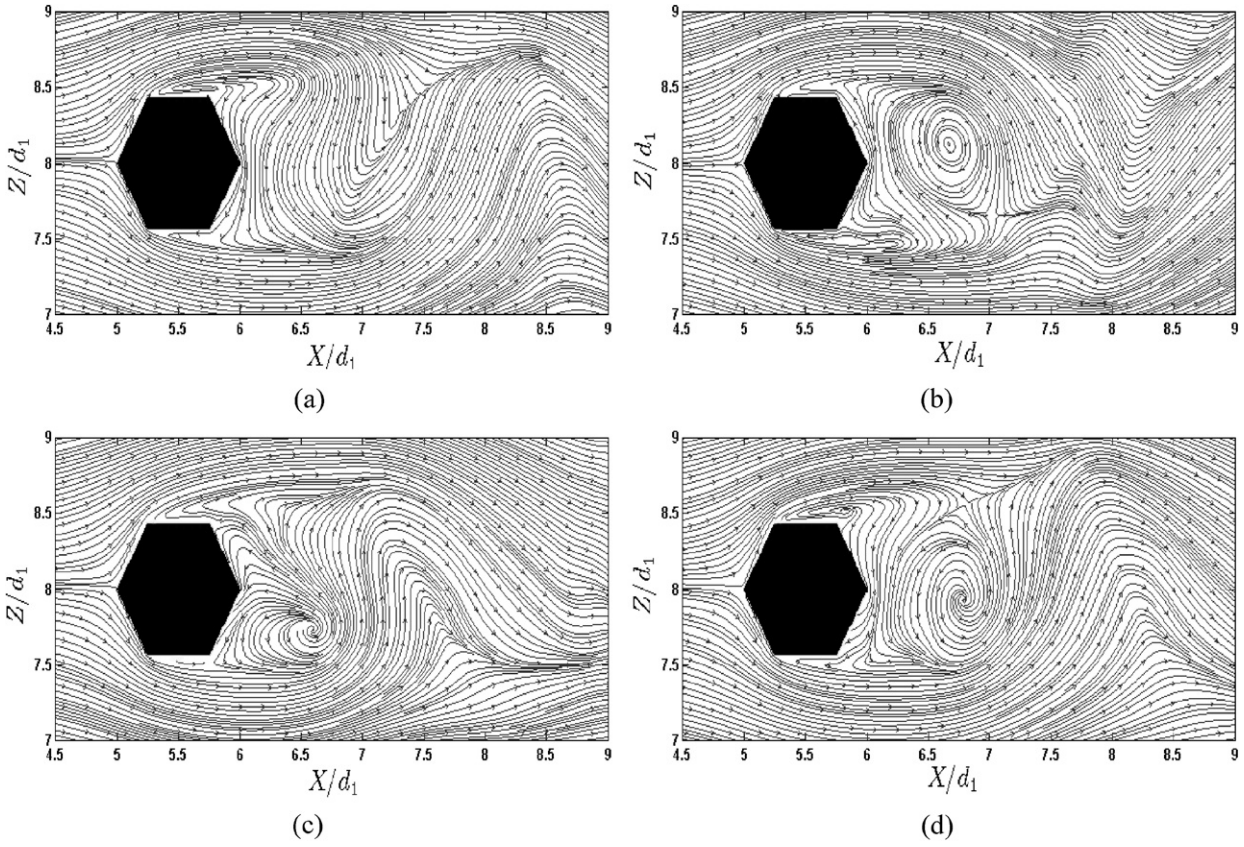

Fig. 9. Instantaneous streamlines of projected velocity vectors into the (X, Z)-plane for flow around the corner-oriented cylinder (A) at $Re = 500$. The plots are separated $1.8d_1/U_0$ in time.

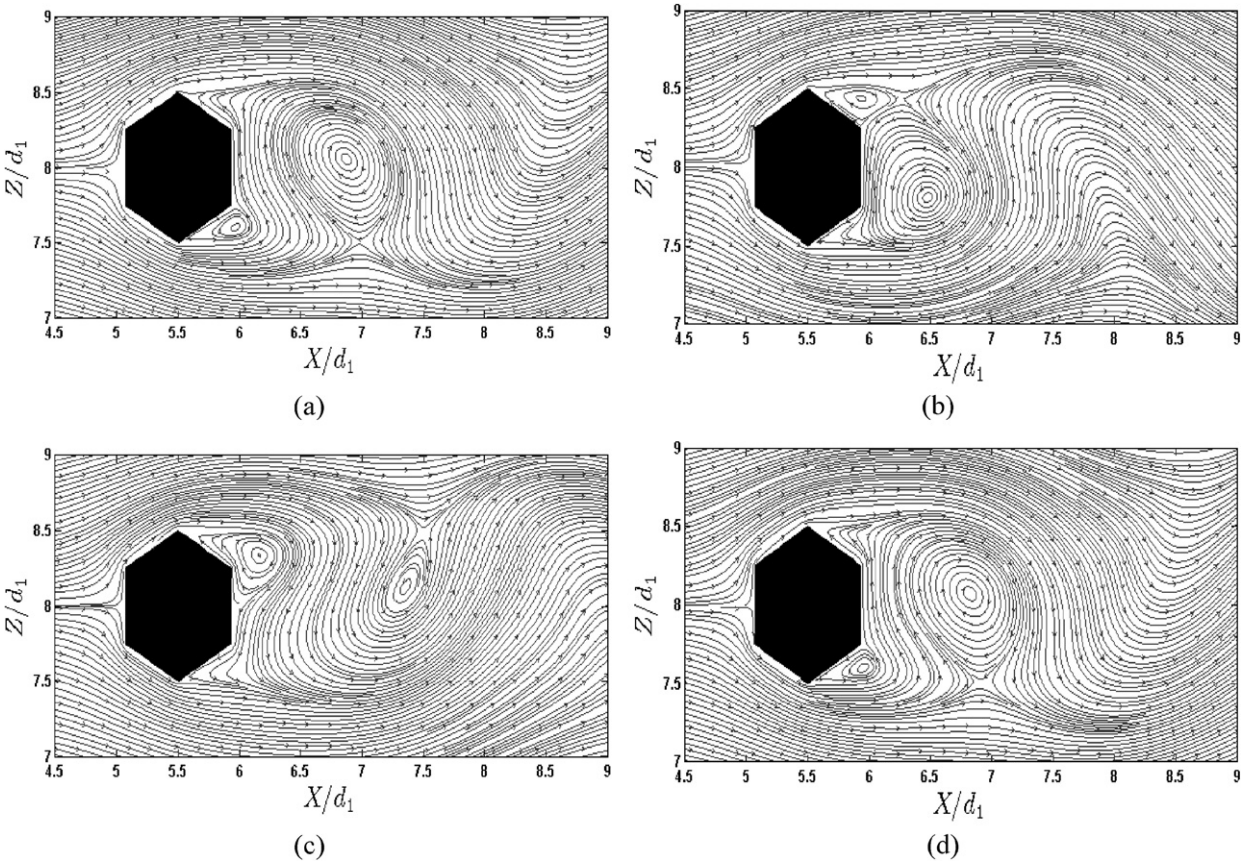

Fig. 10. Instantaneous streamlines for flow around the face-oriented cylinder (B) at $Re = 100$. The plots are separated $1.8d_1/U_0$ in time.

length and velocity scale. While the velocity scale is taken as the free stream velocity U_0, the length scale can be taken either as the height h of the projected cylinder on a plane normal to the free stream or as a geometrical dimension of the cylinder cross-section and thereby independent of the orientation. For a regular polygon with sides d, the distinction between the two choices reduces with the increasing number of sides N. For a square cylinder at 45° incidence, however, the Strouhal number becomes more than 40% larger with the former definition, which also will be adopted herein, i.e. $St \equiv fh/U_0$. Thus, with corner orientation (A) h is the diameter d_2 of the circle inscribed in the hexagonal cross-section. With face orientation (B), on the other hand, h becomes the diameter d_1 of a circle circumscribing the hexagonal cross-section, as shown in Fig. 1. The relevant length scale h is therefore larger with face orientation than with corner orientation of a hexagonal cylinder, contrary to the case of a square cylinder.

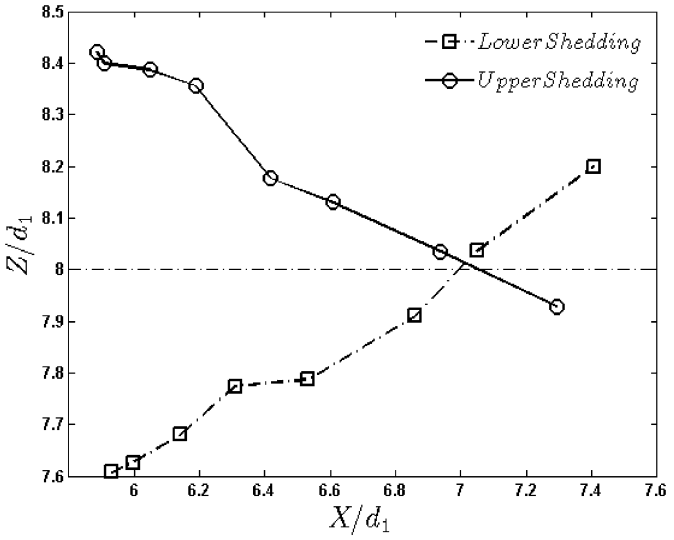

Fig. 11. Trajectories of the vortex centers downstream of the face-oriented cylinder (B) at $Re = 100$.

Data for the Strouhal numbers obtained are presented in Table 1. Irrespective of the orientation of the hexagonal cylinder, a distinct increase in St is observed as the Reynolds number is increased from 100 to 500. Thereafter Re seems to remain the same, at least up to $Re = 1000$. It is a well established fact for wakes behind circular cylinders (Fey et al. [16]) that the Strouhal number increases with Re throughout the parameter range in which the vortex shedding remains two-dimensional. This trend was also found for square cylinder wakes (Sohankar et al. [7]) and for wakes behind other regular polygons with $N \geqslant 6$ by Tian and Wu [15]. At higher Reynolds numbers, however, no discernible Reynolds number effects on St were reported for square cylinder wakes by Vickery [5], Knauss et al. [6], Dutta et al. [11].

For all three Reynolds numbers considered here, the Strouhal number in the case of a face-oriented hexagon (B) is larger than

Table 1
Strouhal numbers in the wake behind a hexagonal cylinder with corner orientation (A) and face orientation (B). The St-numbers refer to the dominating frequency f of the numerically simulated flow field and are accurate to within ±0.0001.

	$Re = 100$	$Re = 500$	$Re = 1000$
Corner orientation A $St = fd_2/U_0$	0.1585	0.1718	0.1718
Face orientation B $St = fd_1/U_0$	0.1831	0.2136	0.2136

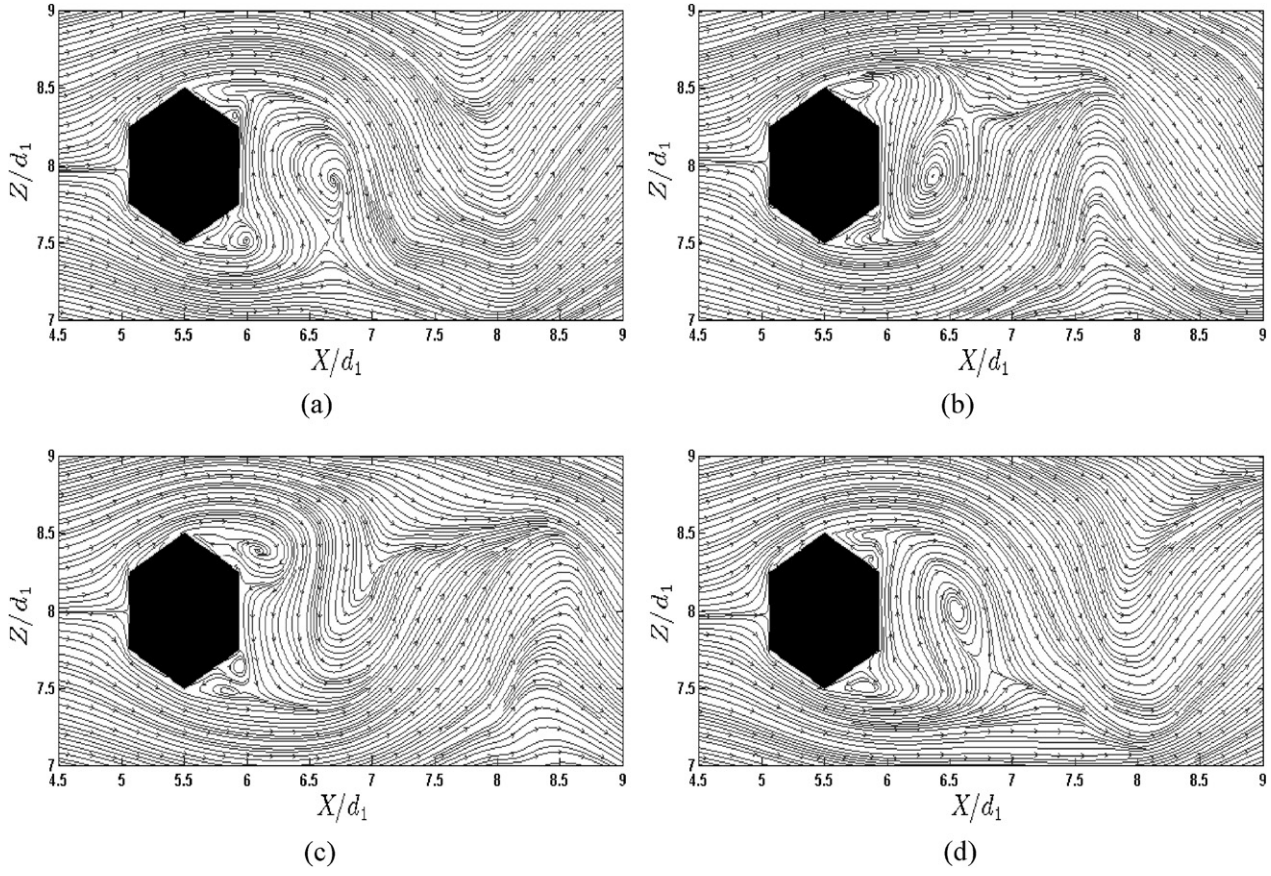

Fig. 12. Instantaneous streamlines of projected velocity vectors into the (X, Z)-plane for flow around the face-oriented cylinder (B) at $Re = 500$. The plots are separated $1.8d_1/U_0$ in time.

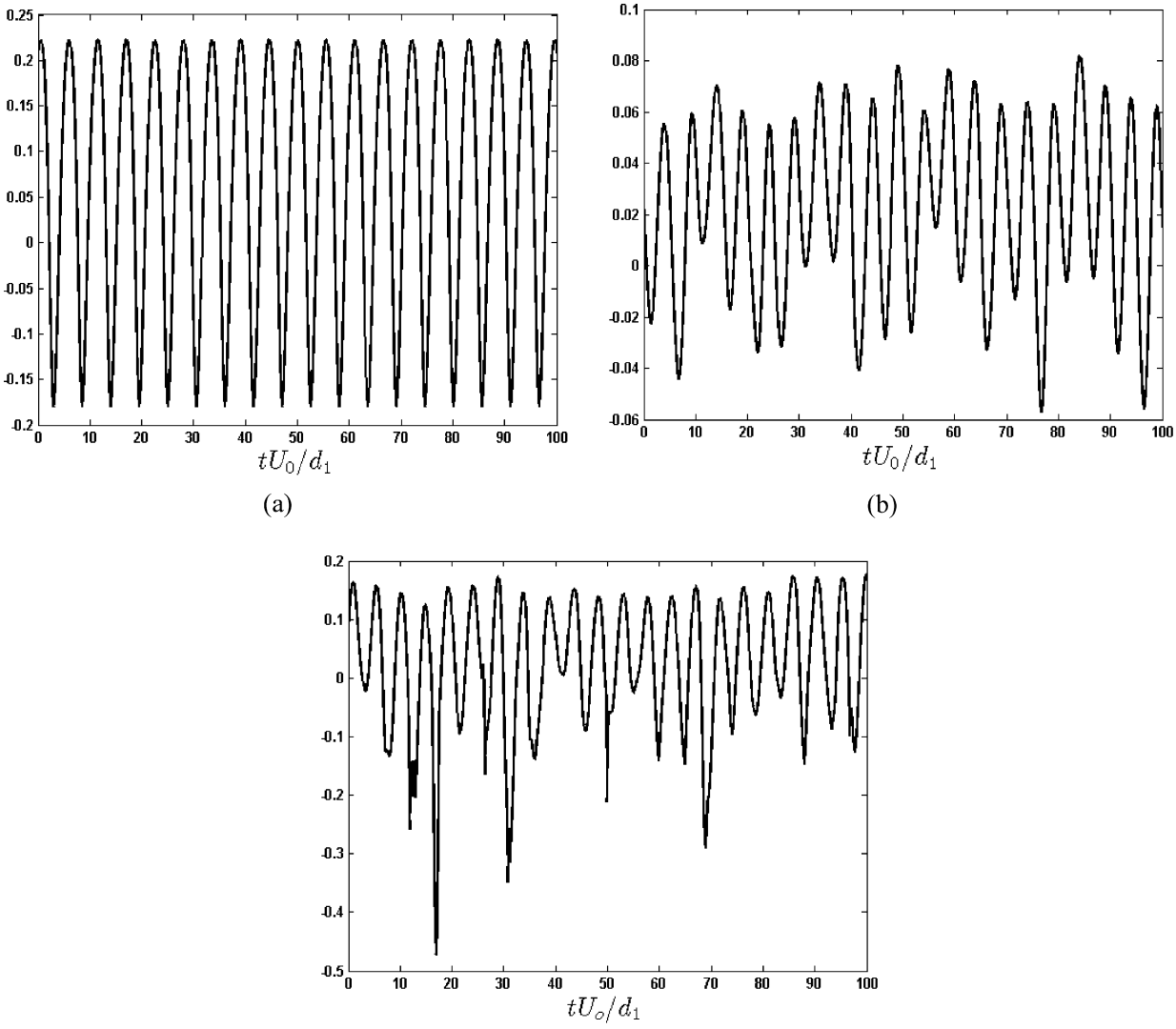

Fig. 13. Time trace of the cross-stream velocity component W monitored at ($X = 9.5d_1$; $Z = 6.5d_1$) in the wake of the hexagonal cylinder with corner orientation (A). (a) $Re = 100$; (b) $Re = 500$; (c) $Re = 1000$.

for the corner-oriented configuration. This contrasts with the earlier findings for square cylinder wakes. As the angle of incidence is increased from zero to 45°, i.e. from face orientation to corner orientation, the Strouhal number is gradually increased such that *St* for a corner-oriented square cylinder is higher than for the side-oriented cylinder.

For a corner-oriented regular polygon, Tian and Wu [15] showed that St decreased with an increasing number *N* of faces and approached the Strouhal number of a circular cylinder in the limit as *N* becomes infinitely large. It should therefore be expected that the Strouhal numbers found for the hexagonal cylinder are somewhat lower than those found for square cylinder wakes. Sohankar et al. [7], however, found that St varied from 0.148 (face orientation) to 0.169 (corner orientation) at a Reynolds number $Re = 100$, whereas the correlation (1) gives $St = 0.165$ for a circular cylinder at the same Reynolds number. The latter value is above the Strouhal number 0.1585 found behind the corner-oriented hexagonal cylinder and is thus apparently in conflict with the anticipations of Tian and Wu [15]. Although not stated explicitly, the Strouhal numbers reported in Ref. [15] are most likely based on the circumscribed diameter d_1 rather than the inscribed diameter d_2. If our *St* in Table 1 is expressed in terms of the circumscribed diameter, *St* becomes 0.1830 for $Re = 100$, i.e. well above that for a circular cylinder.

The wind tunnel study by Bosch and Guterres [14] showed that *St* increased from 0.159 for face orientation to 0.179 for corner orientation of an octagonal cylinder. The Strouhal numbers they reported were based on the inscribed diameter and the Reynolds number was about 5000 (the actual value in their Fig. 14 was not specified). They also showed measured data of the drag coefficient over the entire range of Reynolds numbers considered from 5000 to 20 000 and significantly lower drag was reported for face orientation as compared with corner orientation throughout the Reynolds number range. One can therefore anticipate that the difference in shedding frequency between the two orientations also persists over the entire range of Reynolds numbers. A more relevant Strouhal number for a corner-oriented octagon should instead have been based on circumscribed rather than the inscribed diameter. If so, *St* for corner orientation will be even higher.

3.4. Reynolds-averaged velocity statistics

At the highest Reynolds number considered in the present study, the quasi-periodic vortex shedding co-exists with turbulent

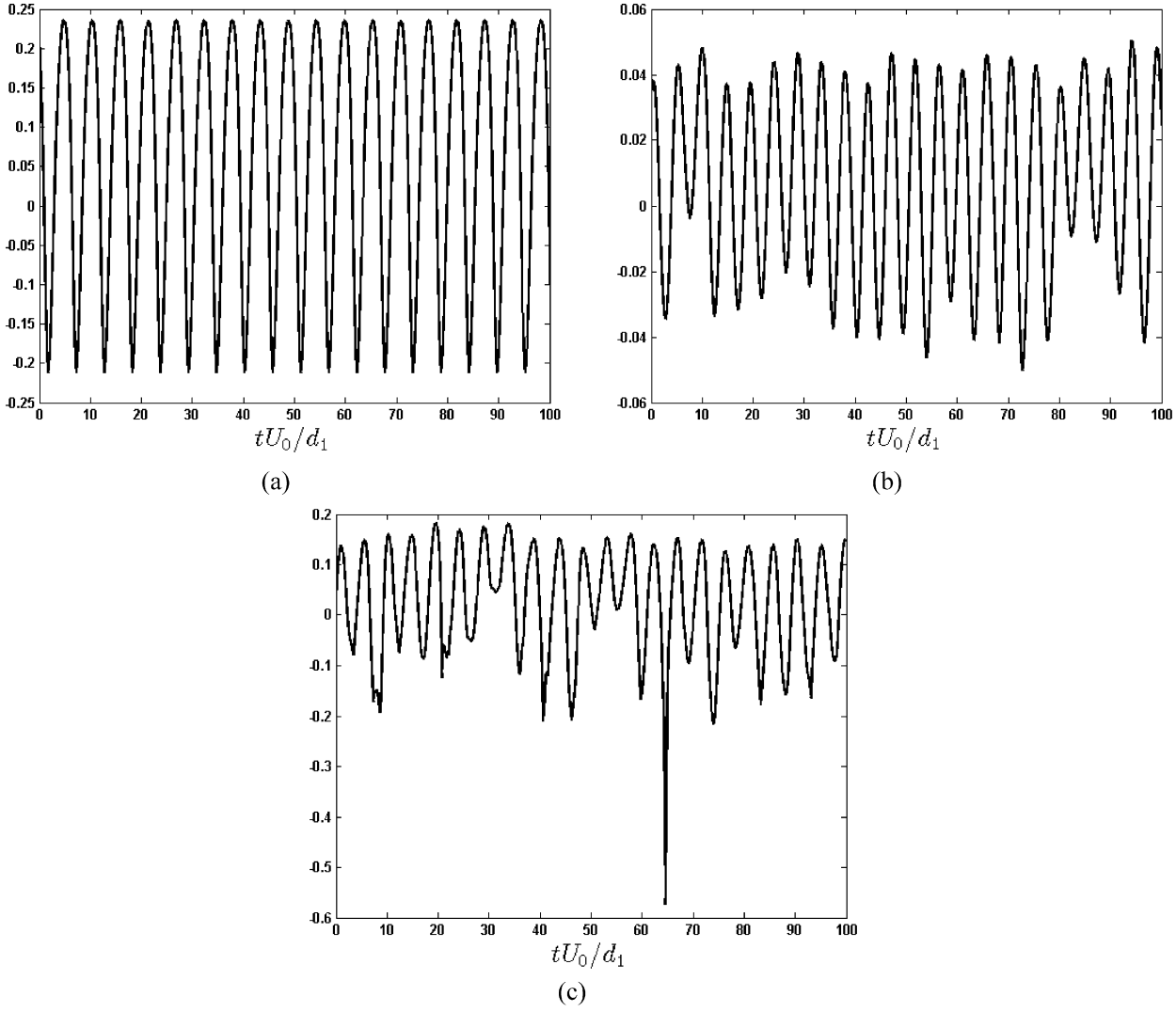

Fig. 14. Time trace of the cross-stream velocity component W monitored at ($X = 9.5d_1$; $Z = 6.5d_1$) in the wake of the hexagonal cylinder with face orientation (B). (a) $Re = 100$; (b) $Re = 500$; (c) $Re = 1000$.

fluctuations of velocity and pressure. The complex unsteadiness of the flow field at $Re = 1000$ is illustrated by the instantaneous vortex topology shown in Figs. 3(a) and 4(a), as well as by the time histories in Figs. 13(c) and 14(c). In this section Reynolds-averaged statistics such as the mean velocity components and the Reynolds-stress components will be presented at $Re = 1000$ for the two different orientations of the hexagonal cylinder. Data have been sampled over $100d_1/U_0$ in time and averaged both in time and in the statistically homogeneous spanwise direction.

Although the flow field is three-dimensional at this Reynolds number, the averaged flow becomes two-dimensional and the streamlines deduced from $\bar{U}$ and $\bar{W}$ are shown in Figs. 15(a) and 15(b) for the corner-oriented and the face-oriented cases, respectively. In both cases a pair of two major recirculation bubbles can be observed in the base region. The length of these bubbles is close to d_1 in both cases and the saddle point (i.e. the location at which the streamwise mean velocity $\bar{U}$ changes sign) is at $X/d_1 = 6.818$ and at $X/d_1 = 6.645$ for the corner- and face-oriented cases, respectively. Although the major separation bubbles are surprisingly similar in the two cases, other aspects of the mean flow field are strikingly different. In the case of corner orientation, the mean flow separates from the leading edge of the flow-parallel faces, whereas the flow separates from the 120° corners when the hexagon is face-oriented. Thus, four faces are affected by mean backflow in the case of corner orientation (A) and only three faces are exposed to flow reversal in the case of face orientation (B). In the latter case, a pair of two smaller recirculating eddies is observed at each of the oblique faces of the hexagonal cylinder. One of these is apparently driven by the large recirculation bubble, whereas the other is driven by the shear layer which separates from the 'shoulder' (i.e. 120° corner) of the hexagon. Since these two smaller eddies recirculate in opposite senses, a stagnation point is established near the center of the oblique rear face. In the case of corner orientation, on the other hand, the trailing end of the flow-parallel faces separates a reversed mean flow along this face from the recirculating flow along the oblique rear face. The flow separation from the leading edge of the flow-parallel plate is qualitatively similar to the flow separation which may occur from the forward corner of a face-oriented square cylinder, as investigated in detail by Lyn and Rodi [21] at $Re = 21\,400$.

In spite of the quasi-periodicity of the instantaneous flow field, Reynolds-averaged statistics give some insight in the local strength of the flow and how it varies in the downstream direction. In the near wake the approximations adopted in classical similarity analysis cannot be justified and only results from full Navier–Stokes simulations provide realistic flow features. Profiles of the mean velocity components $\bar{U}$ and $\bar{W}$ across the wake at three different streamwise locations are shown in Fig. 16. The negative $\bar{U}$ near

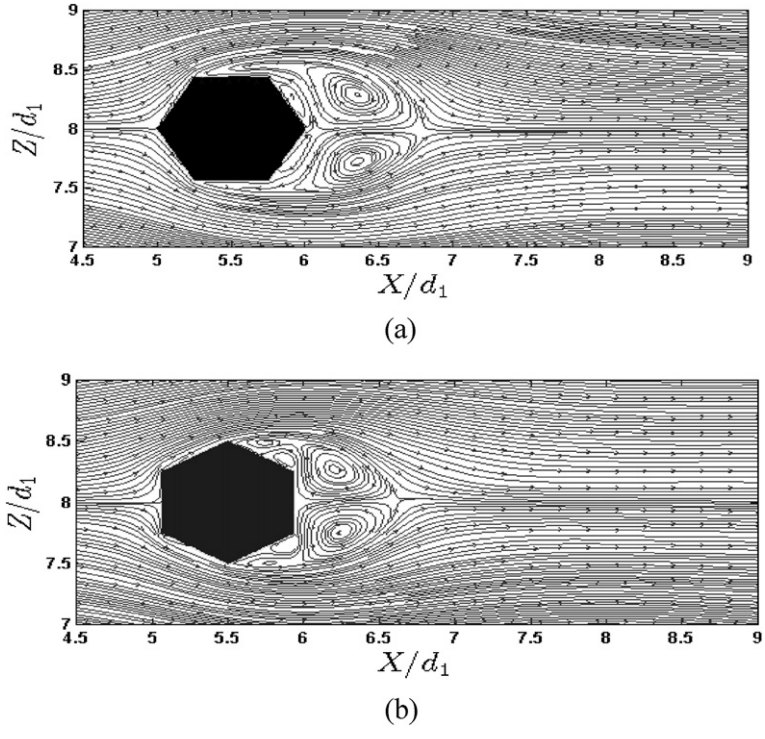

Fig. 15. Streamlines of the mean flow at $Re = 1000$: (a) corner orientation (A); (b) face orientation (B).

the symmetry plane $Z/d_1 = 8$ is due to the mean motion in the upstream direction at $X/d_1 = 6.5$ (see Fig. 15). Here, a substantial velocity overshoot of about 20% just outside the wake arises due the blocking effect of the hexagonal cylinder. Although the width of the projection of the hexagonal cylinder in a plane normal to the flow is larger with face orientation than with corner orientation, a somewhat greater velocity overshoot is observed in the latter case. This is probably because the resulting flow field mimics a more streamlined body with face orientation than with corner orientation. The velocity defect or velocity deficiency reduces rapidly with downstream distance from the body. At $X/d_1 = 11$ the streamwise centerline velocity has recovered to almost $0.6U_0$ and $0.8U_0$ with face and corner orientation, respectively.

The profiles of the cross-stream mean velocity $\bar{W}$ in Figs. 16(c) and 16(d) exhibit the anti-symmetry associated with a symmetric wake flow, i.e. $\bar{W} > 0$ in the lower part of the wake and $\bar{W} < 0$ in the upper part. In the very-near wake or base region, i.e. at $X = 6.5d_1$, the magnitude of $\bar{W}$ is about $0.3U_0$. This fairly high magnitude is associated with the short length of the separation zone and the streamlines are therefore directed towards the symmetry plane of the wake. The cross-stream mean velocity decays rapidly downstream of the separation bubble, as one should expect.

The turbulence intensities or Reynolds stress components are presented in Figs. 17 and 18 for the two different orientations. The streamwise component $\overline{u'^2}$ in Figs. 17(a) and 18(a) exhibits a *bimodal* variation where the two peaks are associated with the mixing-layers on the two sides of the wake. In contrast, the cross-stream component $\overline{w'^2}$ attains its highest value in the core region of the wake. Its maximum value at $X = 6.5d_1$ is almost the same as the peak value of $\overline{u'^2}$, but $\overline{w'^2}$ increases by more than 50% to $X = 7.5d_1$ and eventually starts to reduce.

The velocity fluctuations $\overline{v'v'}$ in the spanwise direction, as shown in Figs. 17(c) and 18(c), are distinctly less energetic than the streamwise and cross-stream fluctuations. The vortex shedding does not contribute directly to the spanwise fluctuations since the shedding is entirely confined to the (X, Z)-plane. In contrast to the two other velocity components, it can therefore be argued that the spanwise velocity fluctuations are associated only with three-dimensionalization of the velocity field due to either wake instabilities or turbulence or both.

The cross-correlation $\overline{u'w'}/U_0^2$ shown in Figs. 17(d) and 18(d) is the only non-zero off-diagonal component of the Reynolds stress tensor. This correlation between streamwise and cross-stream velocity fluctuations exhibits an anti-symmetric variation across the wake, just as the cross-stream mean velocity component. The highest and lowest values of the cross-correlation in the near-wake are associated with the steepest slope of the streamwise mean velocity shown in Fig. 16(a). However, the cross-correlation attains appreciable values in the vicinity of the distinct overshoot of $\bar{U}$ where the mean shear $\partial U/\partial z$ vanishes and an eddy-viscosity based turbulence model will return $\overline{u'w'} = 0$. It is should be pointed out, however, that the cross-correlation $\overline{u'w'}$ as well as the streamwise and cross-stream intensities in Figs. 17 and 18 comprise not only the turbulent velocity fluctuations but also the unsteady part of the velocity field associated with the quasi-two-dimensional vortex shedding. This explains why the cross-stream fluctuations w' are more energetic than the streamwise velocity fluctuations u'.

The profiles of the turbulence intensities and the cross-correlation presented in Figs. 17 and 18 show the same overall behavior as those in found in the near-wake behind other bluff bodies, for instance the wake behind a normal flat plate at $Re = 750$ studied by Narasimhamurthy and Andersson [4]. Moreover, the qualitative features of the profiles of the various intensities turn out to be the same in the case of corner orientation (Fig. 17) and face orientation (Fig. 18).

4. Discussions and concluding remarks

In this Letter we have considered the near-wake of a hexagonal cylinder in cross-flow. Almost no earlier studies have been concerned with this particular cylinder configuration. The only two exceptions we are aware of are the compilation of heat transfer data by Sparrow et al. [13] in which 80-years old measurements of

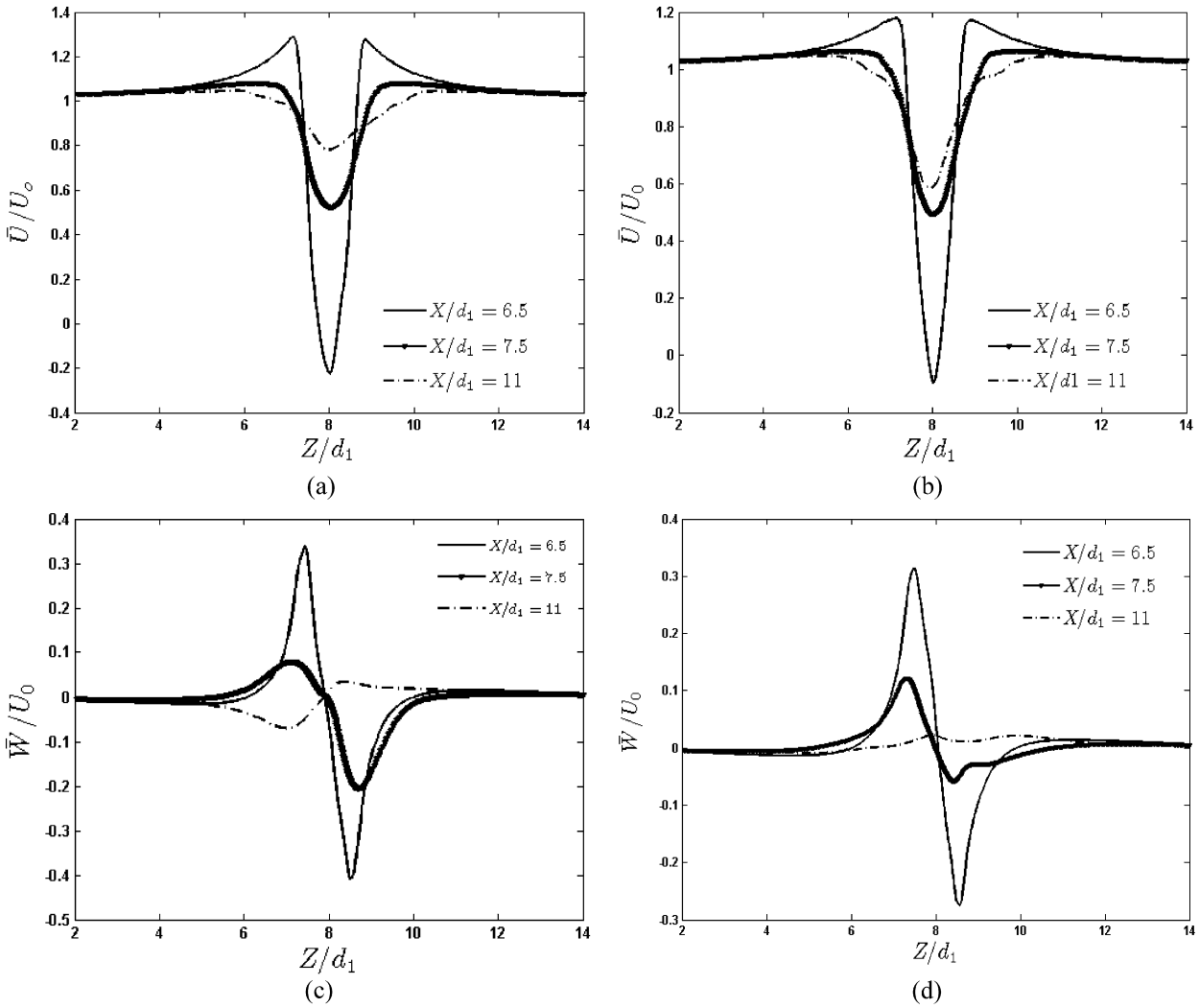

Fig. 16. Mean velocity profiles at fixed X/d_1 positions (the cylinder axis is at $X/d_1 = 5.5$) for $Re = 1000$. Results for corner orientation (A) are to the left and for face orientation (B) to the right. The upper panels show profiles of the mean streamwise velocity and the lower panels show profiles of the mean cross-stream velocity.

the Nusselt number by Hilpert [22] are re-analysed, and the recent CFD-computations by Tian and Wu [15] which were limited to corner orientation and to Reynolds numbers below 80. The influence of the orientation of a hexagonal cylinder relative to the incoming flow on the near-wake flow has never been studied before. Here, flows at three different Reynolds numbers from 100 to 1000 have been considered in order to address Reynolds number effects on the flow separation and vortex shedding frequency.

The Reynolds number referred to in this work was based on the circumscribed diameter d_1 and not on the height h of the projection of the cylinder on a plane normal to the free stream direction. With face orientation of the hexagonal cross-section $h = d_1$, whereas $h = d_2 = 0.866d_1$ for corner orientation. This 14% difference in the value of Re is believed to be of negligible importance as long as the objective is not to pinpoint the critical Reynolds number value at which a transition from one flow regime to another takes place. At this stage, it should be recalled that the critical Reynolds number (based on d_1) for inception of unsteady vortex shedding is $Re_c \approx 48$. It is not known, however, at which Re the periodic two-dimensional wake of the hexagonal cylinder becomes three-dimensional, as observed at $Re = 500$ in Figs. 3(b) and 4(b). For the face-oriented square cylinder, however, Sohankar et al. [8] and Robichaux et al. [23] independently reported that the transition from 2D to 3D shedding occurred between $Re = 150$ and $Re = 200$. A Floquet instability analysis suggested that a long-wavelength (Mode A) disturbance first became unstable at about $Re = 161$ [23].

As far as Reynolds numbers effects are concerned, the strictly periodic vortex shedding at $Re = 100$ turns into a quasi-periodic shedding regime at the higher Reynolds numbers when the regular shedding of spanwise vortices is supplemented with three-dimensional disturbances and eventually by turbulence. The Strouhal number increased as Re was raised from 100 to 500, both for face orientation and corner orientation, in accordance with earlier observations for square cylinder wakes in this Reynolds number range by Sohankar et al. [7]. At moderately high and high Re, on the other hand, no discernible dependence of St on Re was been observed by Dutta et al. [11] and Vickery [5].

Let us recall that not only the Strouhal number but also the Reynolds number can be based on some different length scales. The characteristic dimension used in the original paper by Hilpert [22] on Nusselt–Reynolds-number correlations was the equivalent diameter d_e of a circular cylinder whose perimeter P is equal to that of the non-circular cylinder. Sparrow et al. [13] pointed out errors in the majority of the current heat transfer textbooks incurred by incorrect usage of the characteristic dimension in the Nusselt and Reynolds numbers. As far as hexagonal cylinders are concerned, they reformulated the correlations of Hilpert by using the projected height of the body h rather than the equivalent diameter $d_e = P/\pi = 6d/\pi \approx 1.91d$ originally used by Hilpert [22].

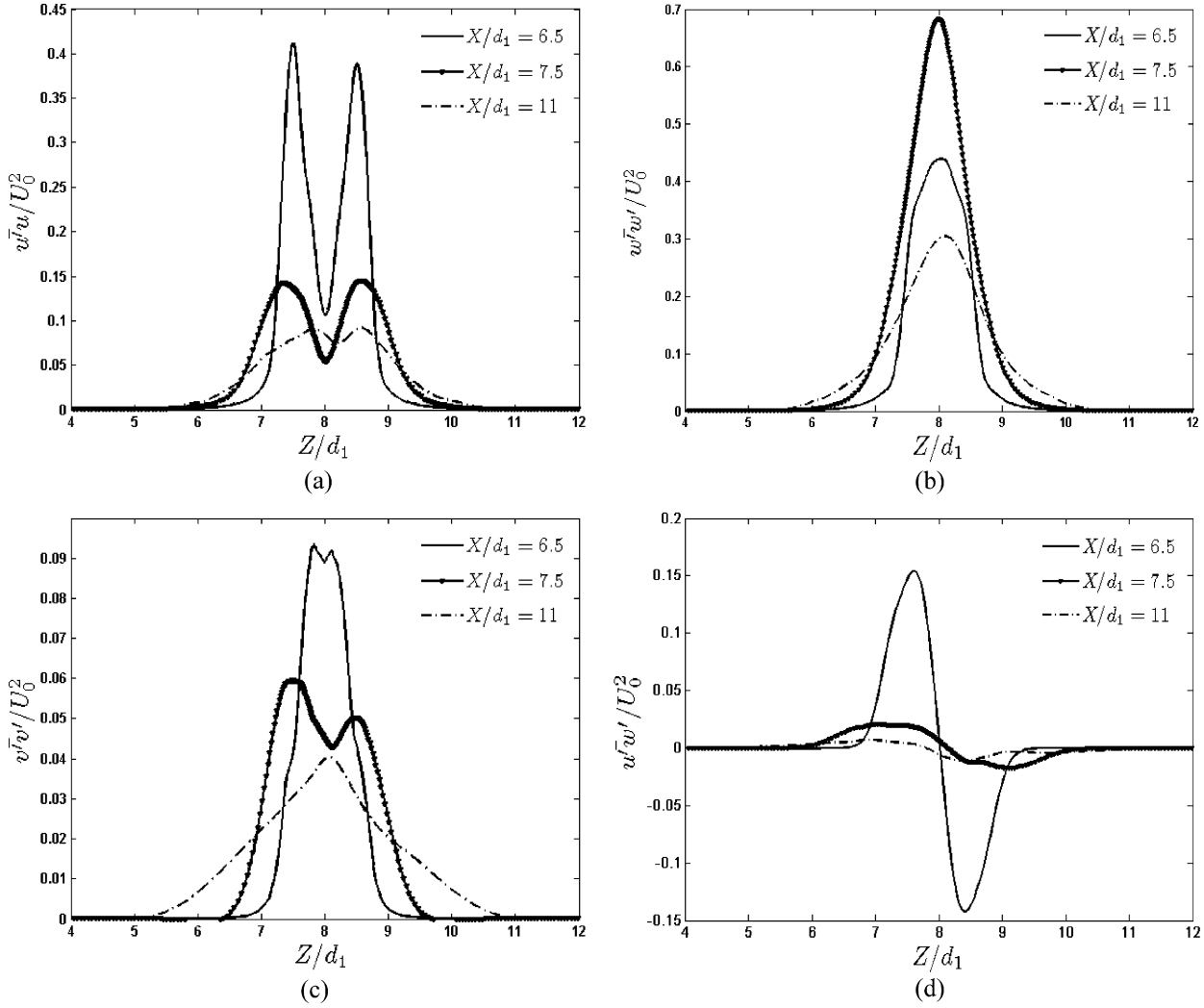

Fig. 17. Turbulence intensities and Reynolds shear stress at fixed X/d_1 positions (the cylinder axis is at $X/d_1 = 5.5$) for $Re = 1000$. Results for corner orientation (A). (a) Streamwise intensities $\overline{u'u'}/U_0^2$; (b) cross-stream intensities $\overline{w'w'}/U_0^2$; (c) spanwise intensities $\overline{v'v'}/U_0^2$; (d) cross-correlation $\overline{u'w'}/U_0^2$.

The Reynolds number *Re* used in the present study was based on the circumscribed diameter $d_1 = 2d$, irrespective of the orientation of the hexagonal cylinder. This Reynolds number is only a factor $2/1.91 \approx 1.047$ larger than the Reynolds number based on the equivalent diameter d_e. A difference in the nominal Reynolds number by less than 5% makes no difference unless a flow transition occurs just in the actual range.

The hexagonal cross-section is that of a regular polygon with an even number of faces ($N = 6$), and it is therefore tempting to anticipate that the resulting wake flow should share some features of the wake behind a square cylinder ($N = 4$) and an octagonal cylinder ($N = 8$). This turned out, however, not to be the case. While an octagonal cylinder resembles a square cylinder in the sense that face orientation implies that two of the faces become aligned with the flow direction, this is not the case for a hexagonal cylinder. In order for two of the faces of the hexagon to be parallel with the main stream, corner orientation is required, as shown in Fig. 1(a). Thus, while an octagon ($N = 8$) probably share features with a square cylinder ($N = 4$), the wake behind a hexagonal cylinder will share its features with a decagonal cylinder ($N = 10$) wake.

The present findings that the Strouhal number is higher with face orientation than with corner orientation are apparently contradictory to the overwhelming number of investigations on the effect of angle of inclination on the wake behind square cylinders. At low Reynolds numbers Sohankar et al. [7] and Knauss et al. [6] found that *St* increased with the angle of attack, i.e. from face orientation to corner orientation, whereas Dutta et al. [11] and Vickery [5] observed the same trend at moderate and high Reynolds numbers, respectively. This apparent contradiction between the present results for the hexagonal cylinder and the earlier results for square cylinders is resolved as soon as face orientation of the square is associated with corner orientation of the hexagon and vice versa. What matters for the wake dynamics is not if the front stagnation point is at a face or a corner, but if the width of the projected cylinder is determined by sharp corners or flow-parallel faces. This new point of view is supported by the experimental data for the wake behind an octagonal cylinder reported by Bosch and Guterres [14], which showed that the Strouhal number increased from 0.16 with face orientation to 0.18 for corner orientation. Just as for the square cylinder, the number of faces of an octagon is 2 times an even number, whereas the number of faces of a hexagon is 2 times an odd number. This is why the same effect of orientation, i.e. face orientation versus corner orientation, is found for the octagon and the square, while the opposite effect is observed for the hexagon.

It is interesting to try to relate the present observations to the 'pre-modern' data for heat transfer by Hilpert [22] as re-analyzed by Sparrow et al. [13]. The average Nusselt number *Nu* for a hexagonal cylinder was higher with face orientation than with corner orientation over a wide range of Reynolds numbers above 5000.

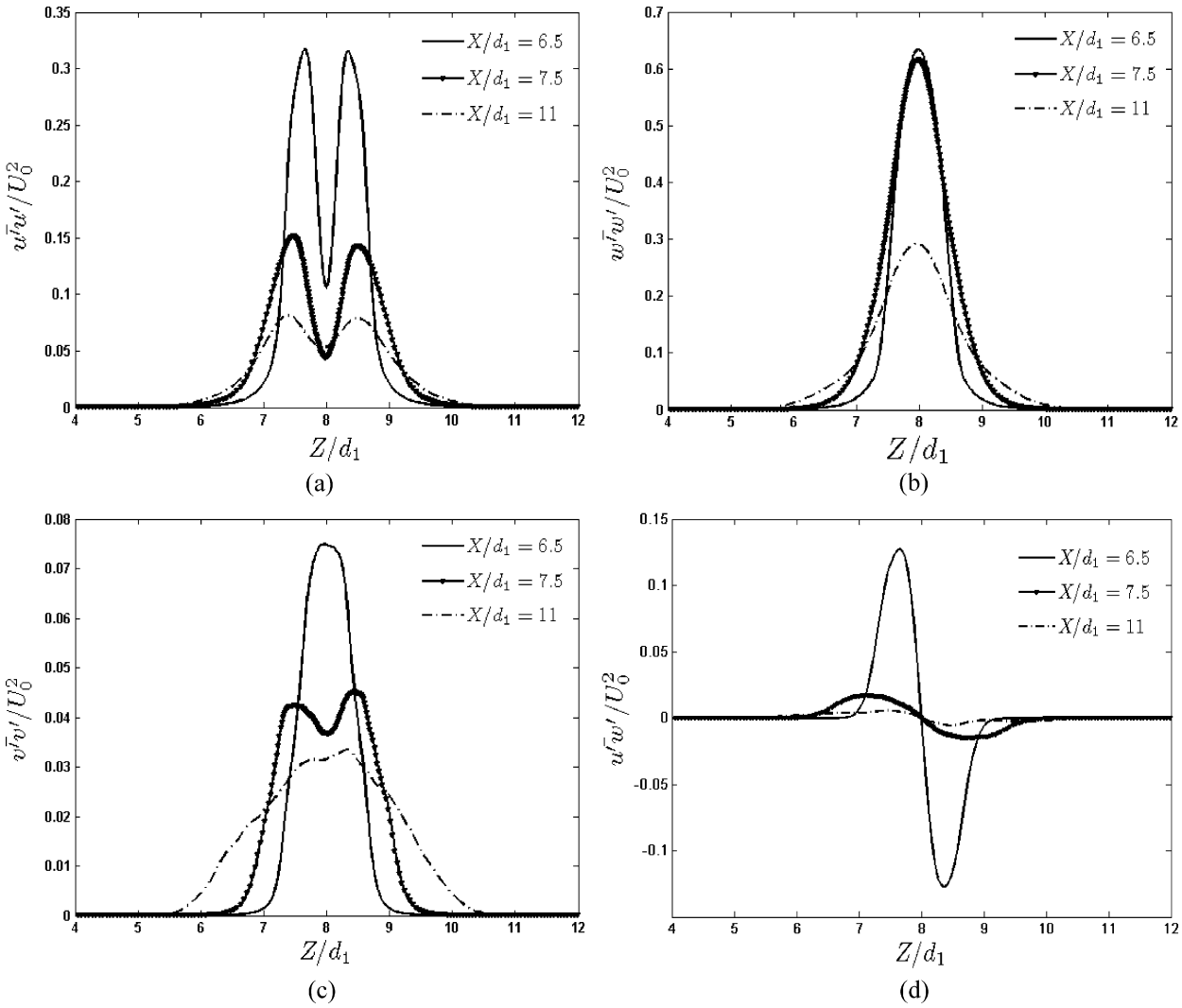

Fig. 18. Turbulence intensities and Reynolds shear stress at fixed X/d_1 positions (the cylinder axis is at $X/d_1 = 5.5$) for $Re = 1000$. Results for face orientation (B). (a) Streamwise intensities $\overline{u'u'}/U_0^2$; (b) cross-stream intensities $\overline{w'w'}/U_0^2$; (c) spanwise intensities $\overline{v'v'}/U_0^2$; (d) cross-correlation $\overline{u'w'}/U_0^2$.

The higher *Nu* with face orientation was attributed to the differences in flow pattern. It was anticipated that five of the six faces was either fully or partially washed by a recirculation zone with face orientation whereas only four of the six faces were supposed to be washed for corner orientation. The measurements of Hilpert [22] could thus be explained by the further assumption [13] that recirculation tended to be enhancing the rate of heat transfer. The flow pattern deduced from the present flow simulations shows, however, that only three of the six faces are washed by regions of recirculation flow for face orientation and four of the faces are washed in the case of corner orientation. The present flow field observed at $Re = 1000$ therefore contradicts with the flow patterns hypothesized to be present above $Re = 5000$ in Ref. [13] in order to explain the influence of the orientation of a hexagonal cylinder on the heat transfer rate. It remains an open question whether or not a fivefold increase of *Re* will alter the topology of the simulated flow field.

Depending on the orientation of the hexagon with respect to the oncoming flow, the flow separates differently from the body and the separated shear layers roll up differently. The streamline patterns for $Re = 1000$ in Fig. 15 suggest that the Karman vortices roll up closer to the body in the case of a face-oriented hexagon and thus results in a shorter formation region and a higher Strouhal number.

The computer simulations show that flow past a *face-oriented* hexagonal cylinder follows the body in the front part and separates from the 120° corners. With this orientation the hexagonal body appears with a blunt frontal area and sharp trailing edges. The boundary layers which develop along the front face and the forward-slanting faces remain attached. This orientation of the hexagonal cylinder therefore corresponds to a corner-oriented square cylinder. Knauss et al. [6] found that the *St–Re* relationship of the corner-oriented square cylinder closely followed the data from a 90° wedge. These observations suggest that the afterbody plays only a minor role.

The *corner-oriented* hexagonal cylinder also exhibited a blunt frontal area, but this comprised only two of the six faces. The boundary layers which developed along the two frontal faces tended to separate at the two faces aligned with the inflow. This phenomenon was observed during parts of the shedding cycle at $Re = 100$ whereas the separation occurred at the leading edge of the flow-parallel faces at the higher Reynolds numbers for which the viscous stresses are reduced relative to fluid inertia. The separated shear layers tend to increase the 'effective' width of the cylinder and thus make the 'effective' Strouhal number higher, i.e. closer to those found for the face-oriented hexagonal cylinder.

In summary one may concluded that the corner-oriented hexagonal cylinder appears as bluffer than it is, just as the

face-oriented square cylinder. The wake dynamics of the corner-oriented hexagon therefore resembles the wake behind a face-oriented square and vice versa.

Acknowledgements

The authors are grateful to the Research Council of Norway for a grant of computation time (Programme for Supercomputing).

References

[1] M.M. Zdravkovich, Flow around Circular Cylinders, vol. 1: Fundamentals, Oxford Scientific Publisher, 1997;
M.M. Zdravkovich, Flow around Circular Cylinders, vol. 2: Applications, Oxford Scientific Publisher, 2003.
[2] C.H.K. Williamson, Annu. Rev. Fluid Mech. 28 (1996) 477.
[3] A. Sohankar, C. Norberg, L. Davidson, J. Wind Eng. Ind. Aerodyn. 69–71 (1997) 189.
[4] V.D. Narasimhamurthy, H.I. Andersson, Int. J. Heat Fluid Flow 30 (2009) 1037.
[5] B.J. Vickery, J. Fluid Mech. 25 (1966) 481.
[6] D.T. Knauss, J.E.A. John, C.H. Marks, AIAA J. Hydronautics 10 (1976) 121.
[7] A. Sohankar, C. Norberg, L. Davidson, Int. J. Numer. Meth. Fluids 26 (1998) 39.
[8] A. Sohankar, C. Norberg, L. Davidson, Phys. Fluids 11 (1999) 288.
[9] A.K. Saha, G. Biswas, K. Muralidhar, Int. J. Heat Fluid Flow 24 (2003) 54.
[10] S.C. Luo, Y.T. Chew, Y.T. Ng, Phys. Fluids 15 (2003) 2549.
[11] S. Dutta, K. Muralidhar, P.K. Panigrahi, Expr. Fluids 34 (2003) 16.
[12] D.-H. Yoon, K.-S. Yang, C.-B. Choi, Phys. Fluids 22 (2010) 043603.
[13] E.M. Sparrow, J.P. Abraham, J.C.K. Tong, Int. J. Heat Mass Transfer 47 (2004) 5285.
[14] H.R. Bosch, R.M. Guterres, J. Wind Eng. Ind. Aerodyn. 89 (2001) 1311.
[15] Z.W. Tian, Z.N. Wu, J. Fluid Mech. 628 (2009) 121.
[16] U. Fey, M. König, H. Eckelmann, Phys. Fluids 10 (1998) 1547.
[17] M. Manhart, Computers & Fluids 33 (2004) 435.
[18] N. Peller, A.L. Duc, F. Tremblay, M. Manhart, Int. J. Numer. Meth. Fluids 52 (2006) 1175.
[19] J. Jeong, F. Hussain, J. Fluid Mech. 285 (1995) 69.
[20] D.A. Lyn, S. Einav, W. Rodi, J.-H. Park, J. Fluid Mech. 304 (1995) 285.
[21] D.A. Lyn, W. Rodi, J. Fluid Mech. 267 (1994) 353.
[22] R. Hilpert, Forsch. Gebiete Ing.-Wesen 4 (1933) 215.
[23] J. Robichaux, S. Balachandar, S.P. Vanka, Phys. Fluids 11 (1999) 560.